J Mater Sci (2009) 44:5557–5562
DOI 10.1007/s10853-009-3778-z

Electrical conductivity, relaxation, and scaling analysis studies of lithium alumino phosphate glasses and glass ceramics

M. V. N. V. D. Sharma · A. V. Sarma · R. Balaji Rao

Received: 25 February 2009 / Accepted: 24 July 2009 / Published online: 6 August 2009

Abstract Different compositions of lithium aluminum phosphate glasses were prepared by melt quenching technique. The best bulk conductivity achieved by the sample G_3, (28 mol% of lithium oxide). Further, the investigation extended by crystallizing the G_3 sample at different temperatures, 200 °C (GC_{200}), 300 °C(GC_{300}), 400 °C (GC_{400}), and 500 °C (GC_{500}). The electrical measurements for all the glasses and glass ceramics were carried out in the frequency range of 1–10^5 Hz and at a temperature range of 393–513 K by the impedance spectroscopy. The variation of conductivity with frequency of the samples was explained in the light of different valency states of aluminum ions. AC conductivity data are fitted to a power law equation. Scaled spectra for ac conductivity and modulus data suggested that the present glass samples follow temperature independent conductivity distribution relaxation mechanism.

Introduction

Lithium aluminum phosphate glasses and glass ceramics consisting of Li^+ ion conductivity have recently become of more interest owing to their technological significance in the recycling of nuclear waste, high energy capacitors, and other electro chromic devices [1–3]. Al_2O_3 is significant electro ceramic material with low values of dielectric loss and dielectric constant has make use of as resonators for ultra stable oscillators in clocks and as substrates. The accumulation of Al_2O_3 in the lithium phosphate glass system extends the glass forming region and reported to occupy both AlO_4 tetrahedral sites and AlO_6 octahedral sites in the glasses that act as network formers and modifiers [4]. Crystalline glass materials or glass ceramics are also possessed interesting properties and exhaustive research is being carried out by a number of researchers [5, 6]. Usually the process of devitrification in crystalline glasses leads to increases in the total conductivity due to elimination of grain boundaries [7]. Further, the investigation is interesting to compare the electrical behavior of glasses and glass ceramics of same sample. Hosono et al. and Minami et al. [8, 9] were reported that crystallized glasses show greater conductivity than the original glasses due to the grain boundaries in few cases. In this study, we focus our attention on the assessment of electrical behavior of glass with crystallized glass at different temperatures of same composition. The electrical properties are projected by the Impedance spectroscopy in view of the fact that this technique is a powerful tool to probe in the glasses and glass ceramics over wide range of temperature and frequency [10, 11].

Experimental

Appropriate amounts of AnalaR grade reagents of Li_2CO_3, Al_2O_3, and P_2O_5 were thoroughly mixed in an agate mortar and thick melted in a platinum crucible at 750 ± 10 °C for about 2 h until a bubble-free liquid was formed. The resultant melt was then cast in a brass mold and subsequently annealed at 350 °C. Glasses of the composition

M. V. N. V. D. Sharma · A. V. Sarma
Department of Physics, Andhra University, Visakhapatnam, Andhra Pradesh 530-003, India

R. Balaji Rao (✉)
Department of Physics, GITAM Institute of Technology, GITAM University, Hyderabad Campus, Hyderabad, Andhra Pradesh 502 329, India
e-mail: ravuri3091@yahoo.co.in

$(20 + x)$ Li_2O–$(20-x)$ Al_2O_3–$60P_2O_5$ ($x = 0$, 4, 8, 12, and 16, in mol%) were prepared by the melt quenching technique and labeled as G_1, G_2, G_3, G_4, and G_5. The amorphous state of the glasses was checked by the X-ray diffraction method. To study crystallization, the bulk glass samples were heat treated in an automatic temperature controlling electric furnace in air at different temperatures (below and above glass transition temperature), respectively, for 5 h. The heating rate was 3 K/min. After heat treatment in the furnace at specified temperature, the samples were sharply chilled in air at room temperature. The samples are crystallized at different temperatures, labeled as GC_{200} (200 °C), GC_{300} (300 °C), GC_{400} (400 °C), and GC_{500} (500 °C). The average values of glass transition temperature (T_g) and the temperature of onset of crystallization (T_c) were evaluated based on the DTA data collected on all the samples.

Results and discussion

The electrical measurements were carried out by impedance spectroscopy, which utilizes alternating current with variable frequency and temperature. When measurements are carried out as a function of frequency and temperature, it is possible to determine the activation energies of the conduction and dielectric relaxation processes [10, 11]. The complex impedance (Z'' vs. Z') plots of all the glass samples were found to exhibit complete semicircles, as depicted in Fig. 1. The bulk resistance (R) for all the samples relative to each experimental temperature is deduced from the intercept of the imaginary Z'' impedance with the real Z' impedance axes, as shown in Fig. 1. The

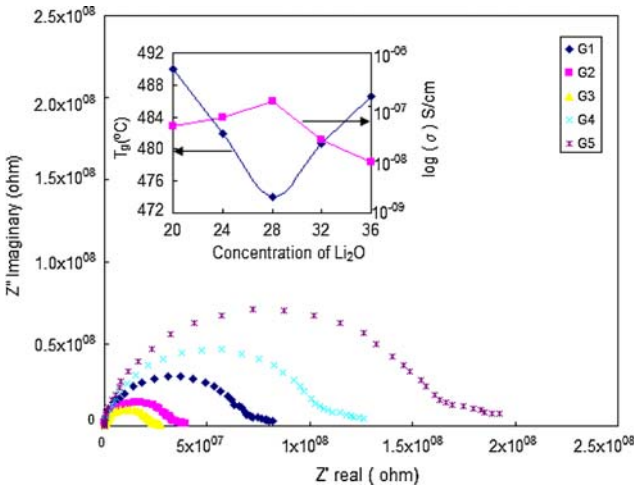

Fig. 1 Impedance spectra Z'' vs. Z' for all the glass samples of lithium alumino phosphate glass system at 403 K. Inset shows variation of glass transition temperature (T_g) and the conductivity log(s) at 403 K with the concentration of Li_2O

bulk conductivity (σ) can be calculated by using the bulk resistance (R) and the pellet dimensions of all the glass samples.

The bulk conductivity (σ) can be calculated by taking the sample geometry into account as follows

$$\sigma = (1/R) \times (t/A) \quad (1)$$

where t/A is the sample geometric ratio, t is the sample thickness and A is the electrode area used to measure the properties of the sample. Using this equation, one can deduce that the highest conductivity is achieved by the G_3 sample (containing 28 mol% of Li_2O) ($\sigma = 1.23 \times 10^{-7}$ S/cm, at 403 K). This is shown in the inset of Fig. 1, where the conductivity of all samples measured at 403 K is plotted as a function of lithium oxide content. From the inset of Fig. 1, it is interesting to note that there appears to be an inverse correlation between the conductivity measured and the glass transition temperature obtained from DTA data.

It is useful to present the ac conductivity of present glasses as function of frequency to evaluate conductivity non-linearities. The dependence of the electrical conductivity with the frequency can be analyzed by the power law equation:

$$\sigma_{(ac)} = \sigma(0) + A\,\omega^s \quad (2)$$

where σ (0) is the conductivity at zero frequency, which is normally termed the dc conductivity, A is a constant and s is a characteristic parameter ($0 < s < 1$). The low frequency part of the conductivity is normally frequency independent and the frequency independent conductivity $\sigma(0)$ is obtained by extrapolation of the conductivity to frequency, $f = 0$. The high frequency part of the conductivity exhibits the dispersion and increases in a power-law fashion [12]. From the inset of Fig. 1, it can be seen that the lowest T_g value for the glass sample (G_3) possesses the highest conducting nature. The reason for the lowest resistivity of G_3 is that the higher concentration of tetrahedrally positioned AlO_4 tetrahedral sites results in a less rigidly bound structure where the Li^+ ions can be blocked by the tetrahedrally positioned aluminum ions. As a result, the conductivity decreases as observed. Hence, the variation of conductivity with the size of the modifier depends on the structural modifications. Typical plots of ac conductivity as a function of frequency at 403 K for all the glasses are presented in Fig. 2. From Fig. 2, it can be seen that the critical frequency ($\omega_p = f_o$), at which the conductivity deviates from the frequency independent part, alter with lithium oxide concentration. The activation energy for conduction ($E_{a\sigma}$) was calculated from the slope of the straight lines obtained when the data are plotted against $1000/T$ of all the glass samples and the composition dependence of activation energy ($E_{a\sigma}$) at 403 K is shown in

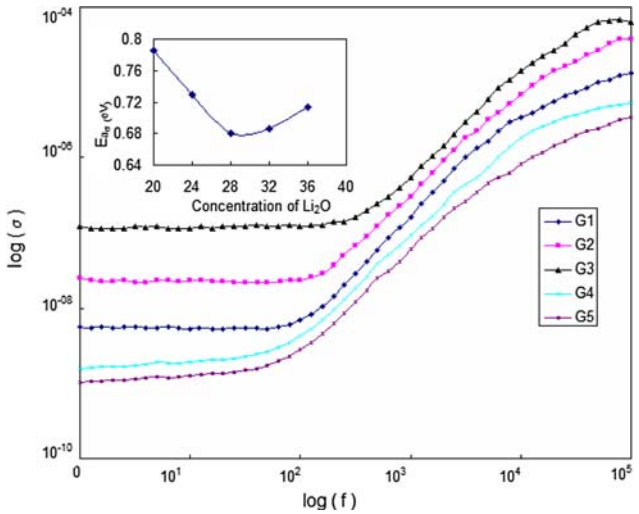

Fig. 2 Log(σ) vs. log(f) plots for all the glass samples of lithium alumino phosphate glasses at 403 K. Inset shows variation of 's' and $E_{a\sigma}$ (eV) with the concentration of Li_2O

the inset of Fig. 2. From the inset of Fig. 2, it is observed that $E_{a\sigma}$ was observed to be lowest for highest conducting G_3 glass sample. The frequency independent part of the conductivity may be attributed due to the long-range transport of Li^+ ions. The frequency dependent part of the conductivity could be explained through diffusion control relaxation method [13].

Further, the investigation is extended by crystallizing the highest conducting sample G_3 at different temperatures viz., 200 °C (GC_{200}), 300 °C(GC_{300}), 400 °C (GC_{400}), and 500 °C (GC_{500}), respectively. In Fig. 3, we show the

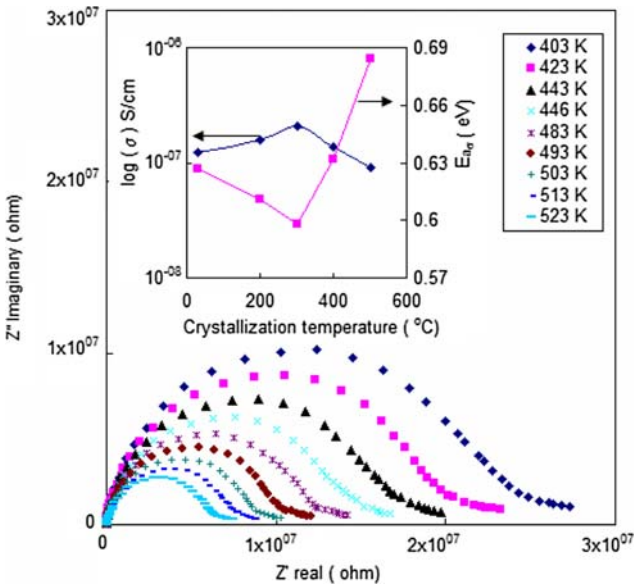

Fig. 3 Impedance spectra Z'' vs. Z' of highest conducting sample crystallized under 300 °C(GC_{300}), measured at different temperatures (403–513 K). Inset shows variation of log σ and $E_{a\sigma}$(eV) with the crystallization temperature at 403 K

characteristic complex impedance plots at different temperatures for the glass ceramic sample (GC_{300}), where it can be seen that increase in temperature caused the impedance semicircles to be shifted to lower and lower Z' values. Once again, one can use the intersection points of the imaginary impedance onto the real axis of semicircles to use Eq. 1 to calculate the bulk conductivity as a function of temperature. The bulk conductivities calculated from the analyzed impedance data obtained at 403 K for all the glass ceramics samples and for the highest conducting glass ceramic sample GC_{300}, at different temperatures are plotted in Figs. 4 and 5. The conductivity data are fitted to the Arrhenius equation

$$\sigma_{dc} = \sigma_0 \exp(-E_{a\sigma}/kT) \quad (3)$$

where σ_0 is the pre exponential factor and $E_{a\sigma}$, k, and T are the activation energy for the conduction, Boltzman's constant, and absolute temperature, respectively. The variation of conductivity and activation energy for conduction ($E_{a\sigma}$) with crystallization temperature at 403 K is shown in the inset of Fig. 3. In the inset of Fig. 3, it is observed that the conductivity is highest and the activation energy (Table 1) is lowest for the sample crystallized at 300 °C (GC_{300}). Since the inset of Fig. 3 (activation energy ($E_{a\sigma}$), versus crystallization temperature) does not show the non-linear behavior of conductivity; the non-linearity between the conductivity and the activation energy suggests that the conductivity enhancement is directly related to nucleation capacity and the decrease in the conductivity from GC_{300} to GC_{500} is expected due to massive crystallization [14].

Another approach to probe the electrical response of materials containing some degree of ionic conductivity is

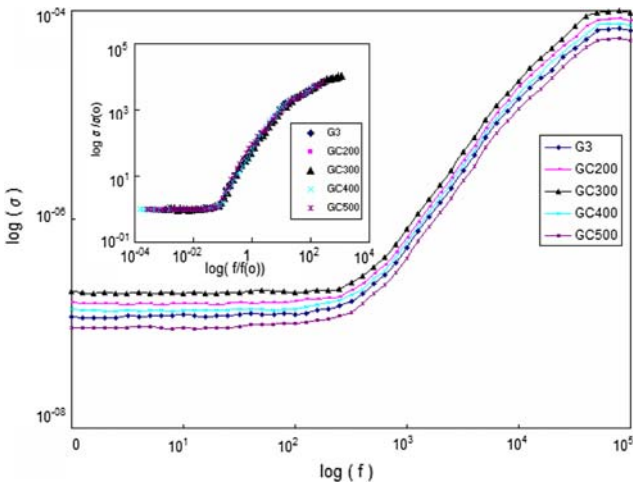

Fig. 4 Log(σ) vs. log(f) plots for all the glass ceramic samples crystallized at 30 °C (G_3), 200 °C (GC_{200}), 300 °C (GC_{300}), 400 °C (GC_{400}), and 500 °C (GC_{500}) at 403 K. Inset shows the scaled spectra of conductivity for all the samples crystallized under different temperatures at 403 K

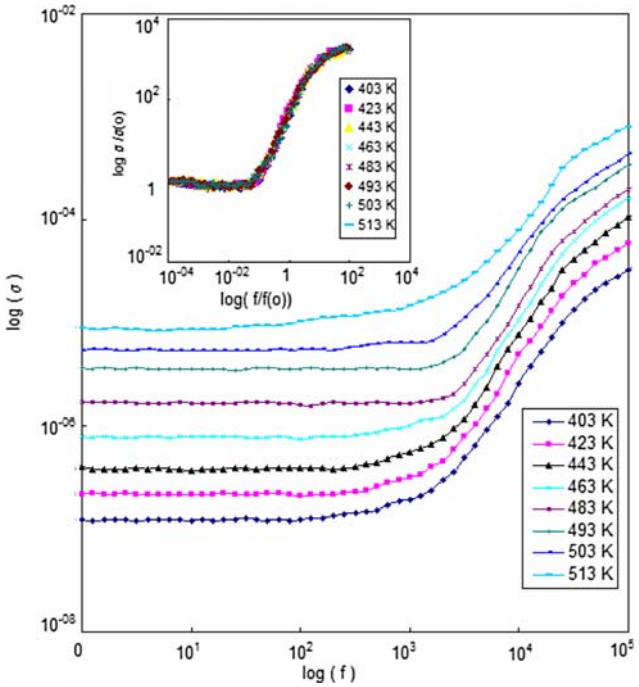

Fig. 5 Log(σ) vs. log(f) plots for highest conducting sample crystallized under 300 °C (GC_{300}) at different temperatures (403–513 K). Inset represents log($\sigma/\sigma(0)$) vs. log($f/f(0)$) for the GC_{300} sample measured at 403–513 K

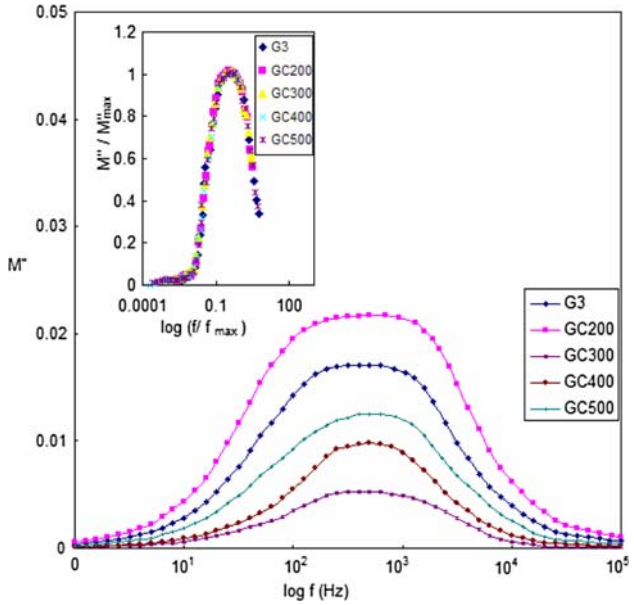

Fig. 6 Electric modulus M'' vs. log(f) for all the glass ceramic samples of lithium alumino phosphate glasses measured at 403 K. Inset shows M''/M''_{max} vs. the log(f/f_{max}) plots for all the samples crystallized at different temperatures at 403 K

to use the complex electric modulus $M^*(\omega) = M' + jM''$ formalism, where M' is the real part of the electric modulus and M'' is the imaginary part of electric modulus. This formulation has been used to identify phenomena as electrode polarization and bulk phenomena such as average conductivity relaxation times τ_σ [15–17].

The complex electrical modulus M^* is related to the complex impedance as described in the equation below:

$$M^*(\omega) = j\omega C_0 Z^*(\omega) \tag{4}$$

where C_0 is the geometric capacitance of the cell, ω is the angular frequency, and $j = \sqrt{-1}$. The dependence of electric modulus on frequency is given by

$$M^*(\omega) = \frac{1}{\varepsilon_s}\left[1 - \int_0^\infty \mathrm{d}t \exp(-j\omega t)\left(-\frac{\mathrm{d}\phi}{\mathrm{d}t}\right)\right], \tag{5}$$

where ε_s is the dielectric constant at high frequency limit and ϕ(t) is the relaxation function. The variation in the imaginary part of electric modulus M'' with the frequency obtained for all the glass ceramic samples at 403 K is shown in Fig. 6. Figure 7 shows the imaginary part of electric modulus M'' dependence with frequency for the highest conducting glass sample GC_{300} at different temperatures. The M'' values show typically asymmetric peaks, which are representative of the nature of the relaxation behavior. This relaxation behavior and the skew nature of the M'' curves with the variation of crystallization temperature obviously suggest the impenetrability of inter–ionic interactions due to the existence of a large number of non-bridging oxygens in the vicinity. It can be observed that the M'' value is observed to be constant (M''_{max}) at a relaxation frequency (f_{max}) and the peak M''_{max} symmetrically shifts toward higher frequencies with increasing temperatures. From Fig. 6, the relaxation frequency (f_{max}) corresponding to the

Table 1 Summary of activation energy ($E_{a\sigma}$), activation energy for conductivity relaxation ($E_{a\tau}$ (eV)), characteristic parameter (s), relaxation time (τ), and critical frequency (f_0) for the crystallized glass samples at different temperatures measured at 403 K

Crystallized sample	$E_{a\sigma}$ (eV)	$E_{a\tau}$ (eV)	s (403 K)	$\tau \times (10^{-4}$s) (403 K)	f_0 (kHz) (403 K)
G_3	0.627	0.631	0.677	1.52	1.42
GC_{200}	0.611	0.624	0.666	1.61	1.38
GC_{300}	0.598	0.609	0.645	2.23	1.23
GC_{400}	0.632	0.643	0.679	1.29	1.11
GC_{500}	0.684	0.698	0.686	1.10	1.01

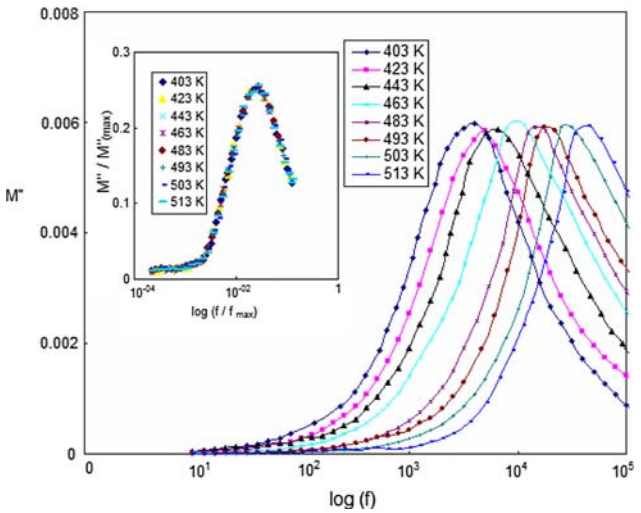

Fig. 7 Electric modulus (M'') vs. log(f) plots obtained at different temperatures at 403–513 K of high conducting sample (GC_{300}). Inset shows M''/M''_{max} vs. the log(f/f_{max}) plots for the GC_{300} sample measured at different temperatures (403–513 K)

maximum in M'' curves and the relaxation time (τ) for all the glass ceramics samples at 403 K is calculated using the relation $\tau = 1/2\pi\ f_{max}$ can be obtained and tabulated in Table 1. The experimental data are well described by the Arrhenius expression, given as below:

$$\tau = \tau_0 \exp(E_{a\tau}/kT) \quad (6)$$

where τ_0 is the pre-exponential factor and $E_{a\tau}$ is the activation energy for conductivity relaxation.

Scaling analysis is to demonstrate that the mechanism of ion transport in the glasses or glass ceramics is unaffected by composition and temperature of various glass ceramic samples collapse in to single super curve [15–18]. In the scaling spectra, ac conductivity data obtained at various temperatures are scaled with critical frequency (f_0) and the frequency independent conductivity $\sigma(0)$ of the frequency axis (x axis) and ac conductivity axis (y axis) [18, 19]. Scaled spectra of conductivity ($\log(\sigma/\sigma_0)$ vs. $\log(f/f_0)$) for all the glass ceramic samples (Inset of Fig. 4) at 403 K propose that the dispersion in the conductivity relaxation mechanism expected not only due to the bond strength of Li^+ with the surrounding ions, but also due to the concentration of octahedral sites of Al^{3+} ions, which acts as network modifiers in the glass matrix. Scaled conductivity curves at different temperatures ($\log(\sigma/\sigma_0)$ vs. $\log(f/f_0)$) (Inset of Fig. 5) collapse into a single super curve; this single super curve suggests that the present glass samples show evidence of the temperature independent conduction transport mechanism based on time-temperature superposition principle [19, 20]. Inset of Fig. 6 shows the scaled spectra of electric modulus (M''/M''_{max} vs. $\log(f/f_{max})$ for all the samples crystallized at different temperatures at 403 K. The divergence in the scaled spectra suggests that the relaxation time dependent on the structure of the glass matrix, contiguous surroundings of Li^+ ions, and octahedral sites of Al^{+3} ions, which act as network modifiers in the glass ceramic matrix. The scaled spectra of electric modulus (M''/M''_{max} vs. $\log(f/f_{max})$) at different temperatures collapse into single super curve, which is shown in the inset of Fig. 7. This behavior in the present crystallized samples at different temperatures suggests that the frequency dependent relaxation process is temperature independent.

Conclusions

The variation of ionic conductivity with crystallization temperature is due to tetrahedral (network former) and octahedral sites (network modifier) of aluminum ions in the present glass ceramics samples. The highest conductivity ($\sigma = 2.070 \times 10^{-7}$ S/cm) for glass ceramic sample (GC_{300}) measured at 403 K is due to the octahedral aluminum ions, which act as net work modifiers. The ac conductivity data fitted to a power law equation. The activation energy for conduction and power exponent's' were calculated to be 0.598 eV, 0.645 for the highly conducting sample GC_{300}. Single super curve in the scaled spectra of the conductivity and electric modulus suggests evidence of the temperature independent conduction transport mechanism and distribution relaxation time mechanism with the present glass ceramic samples. The activation energies calculated from the conductivity curves and those of the relaxation were essentially the same (Table 1). This suggests that the present glass ceramic samples exhibit single conduction mechanism.

References

1. Abrahams I, Hadzifejzovic E (2000) Solid State Ionics 134:249
2. Du J, Jones B, Lanagan M (2005) Mater Lett 59:2821
3. Gao Z, Drummond CH (1999) J Am Ceram Soc 82(3):561
4. Muller D, Ladwig G, Hallas E (1983) Phys Chem Glass 24:37
5. Saito T, Tatsumisago M, Minami T (2001) J Ceram Soc Jpn 109:757
6. El-Batal HA, Azooz MA (2001) Indian J Pure Appl Phys 39:565
7. Aono H, Sugimoto E, Adachi G (1989) J.Electrochem Soc 136:590
8. Hosono H, Abe Y (1991) Solid State Ionics 44:293
9. Minami T, Machid N (1992) Mater Sci Eng B 13:203
10. Balaji Rao R, Gerhardt RA (2008) Mater Chem Phys 112(1):186
11. Foltyh MF, Wasiucionek M, Nowinski JL (2005) Solid State Ionics 176:2137
12. Nobre MAL, Lafendri S (2001) J Phys Chem Solids 62:1999
13. Elliot SR, Owens AP (1994) Solid State Ionics 70:27

14. Gedam RS, Deshpande VK (2006) Solid State Ionics 177:2589
15. Funke K, Banhatti RD (2004) Solid State Ionics 169:1
16. Schroeder TB, Dyre JC (2000) Phys Rev Lett 84:310
17. Roling B (1998) Solid State Ionics 105:185
18. Sidebottom DL (1999) Phys Rev Lett 82:3653
19. Ghosh A, Pan A (2000) Phys Rev Lett 84:2188
20. Muralidharan P, Satyanarayana N, Venkateswarlu M (2005) Phys Chem Glass 46:293